Quantitative determination of interlayer electronic coupling at various critical points in bilayer MoS$_2$

Wei-Ting Hsu [1,7,*] Jiamin Quan,[1,*] Chi-Ruei Pan [2] Peng-Jen Chen,[2,3] Mei-Yin Chou,[2] Wen-Hao Chang [4,5]
Allan H. MacDonald,[1] Xiaoqin Li,[1] Jung-Fu Lin [6] and Chih-Kang Shih [1,7,†]

[1]*Department of Physics, The University of Texas at Austin, Austin, Texas 78712, USA*
[2]*Institute of Atomic and Molecular Sciences, Academia Sinica, Taipei 10617, Taiwan*
[3]*Institute of Physics, Academia Sinica, Taipei 11529, Taiwan*
[4]*Department of Electrophysics, National Yang Ming Chiao Tung University, Hsinchu 30010, Taiwan*
[5]*Research Center for Applied Sciences, Academia Sinica, Taipei 11529, Taiwan*
[6]*Department of Geological Sciences, Jackson School of Geosciences, The University of Texas at Austin, Austin, Texas 78712, USA*
[7]*Department of Physics, National Tsing Hua University, Hsinchu 30013, Taiwan*

Tailoring interlayer coupling has emerged as a powerful tool to tune the electronic structure of van der Waals (vdW) bilayers. One example is the usage of the "moiré pattern" to create controllable two-dimensional electronic superlattices through the configurational dependence of interlayer electronic couplings. This approach has led to some remarkable discoveries in twisted graphene bilayers, and transition metal dichalcogenide homo- and heterobilayers. However, a largely unexplored factor is the interlayer distance d, which can impact the interlayer coupling strength exponentially. In this paper, we quantitatively determine the coupling strengths as a function of interlayer spacing at various critical points of the Brillouin zone in bilayer MoS$_2$. The exponential dependence of the coupling parameter on the gap distance is demonstrated. Most significantly, we achieved a 280% enhancement of K-valley coupling strength with an 8% reduction of the vdW gap, pointing to a strategy for designing a unique electronic system in vdW bilayers.

I. INTRODUCTION

In the current topic of van der Waals hetero- and homobilayers, the interlayer electronic coupling plays a critical role in determining the electronic structures of the bilayer as a whole [1–7]. Active control of interlayer coupling through moiré superlattices (MSLs) has emerged as a powerful tool for tailoring electronic structures in twisted bilayer graphene and transition metal dichalcogenides (TMDs) [8–24]. This approach utilizes the formation of periodic modulation of in-plane alignment between the two atomic sheets (either by twisting angle or lattice mismatch) to engineer a periodically modulated moiré potential. Another less explored, but potentially fruitful direction, is to control interlayer coupling through interlayer distance. This approach can be used alone or in combination with moiré superlattice (MSL) formation to enhance its functionalities, as demonstrated in twisted bilayer graphene [8–10,21]. For interlayer coupling, although the effect of in-plane stacking configuration is well understood [19,20], the out of plane effect due to the change in interlayer spacing is more difficult to capture quantitatively. More significantly, there is evidence that changes in local interlayer spacing can be substantially different from density functional theory (DFT) calculations [6]. Thus, an independent experimental determination of the interlayer coupling as a function of interlayer spacing would play an important role in assessing the theoretical model for predicting the electronic structures. Such a quantitative determination will enable a design parameter to tailor the electronic structure of van der Waals (vdW) bilayers through interlayer spacing control [21–24].

In this work, by using 2H-stacked bilayer MoS$_2$ (without MSL effect) as a model system, we report quantitative determination of interlayer coupling strength as a function of the interlayer spacing at different critical points of the Brillouin zone. The usage of 2H-stacked bilayer MoS$_2$ removes fabrication uncertainties associated with mechanical stacking of bilayers [18,25], making the data interpretation and extraction of coupling energy more straightforward. It also removes the lateral configuration variations in a MSL and allows one to assess the coupling as a function of layer spacing independently. By applying hydrostatic pressure in a diamond anvil cell up to 12.7 GPa, the interlayer spacing is changed from 0.62 to 0.57 nm, representing an 8% change. The coupling strength at various critical points is probed using a combination of differential reflectivity (DR) and photoluminescence (PL) spectra from which the exponential decay constants of the interlayer coupling at different critical points are determined. We further compare the results with the *ab initio* calculations and find that all the results of K, Q, and Γ points agree well with the DFT calculations. Importantly, after reducing the interlayer distance by 8%, the K-valley coupling strength is enhanced

*These authors contributed equally to this work.
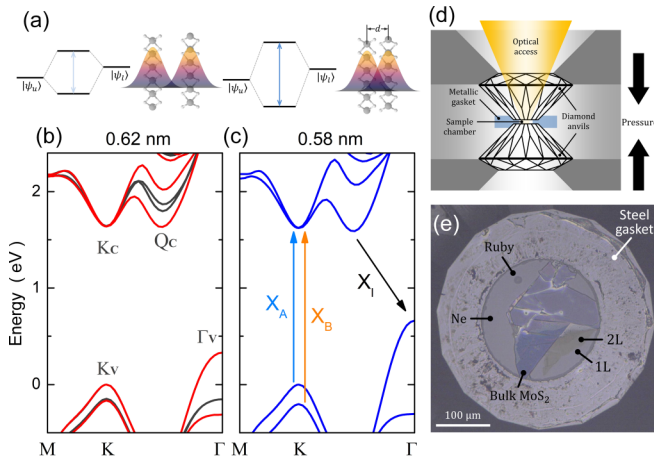†shih@physics.utexas.edu

125302-1

FIG. 1. Control of interlayer electronic coupling using high-pressure diamond anvil cell. (a) Schematic showing the interlayer hybridization of $|\psi_u\rangle$ and $|\psi_l\rangle$. When the interlayer spacing d decreases, the orbital wave function overlap increases, which enhances the coupling strength and leads to larger energy splitting of the hybridized state. (b), (c) DFT band structure of monolayer MoS_2 (black) and bilayer MoS_2 with interlayer spacing $d = 0.62$ nm (red) and 0.58 nm (blue). At the Γ_V, Q_C, and K_V points, band splitting becomes larger for a bilayer with a smaller d. (d) Schematic showing a diamond anvil cell that can be accessed by optical spectroscopy. (e) An optical image showing the monolayer (1L), bilayer (2L), and bulk MoS_2 loaded in the high-pressure chamber. A ruby sphere is used as a pressure calibrant with the Ne medium loaded in the chamber (see Supplemental Material [35]).

from 36 to 101 meV, representing a 280% enhancement. This result also points to a very promising strategy for designing novel quantum structures based on vdW bilayers.

II. RESULTS AND DISCUSSION

Conceptually, the interlayer electronic coupling in vdW bilayers can be described by a 2×2 Hamiltonian $H = \begin{bmatrix} \varepsilon_l & -t \\ -t & \varepsilon_u \end{bmatrix}$, where ε_l (ε_u) is the single-particle energy level of the lower (upper) layer prior to coupling and t is the coupling strength (also referred to as the interlayer hopping integral). A larger coupling strength t and/or a smaller energy difference ($\varepsilon_l - \varepsilon_u$) can lead to a larger energy splitting of the hybridized states. This model was successfully applied recently to capture the interlayer hybridization in commensurate heterobilayers [20]. Crucially, the coupling strength t depends on several factors, i.e., the stacking configuration [19,20], the interlayer spacing d, and the critical point of the Brillouin zone. Due to the different projected atomic orbitals at different critical points, one expects to observe different coupling strengths at different valleys. Furthermore, when the interlayer spacing d decreases, the increased orbital wave function overlap enhances the coupling strength t and results in a larger energy splitting of the hybridized states, as depicted by the schematic shown in Fig. 1(a).

In bilayer MoS_2 [26–28] and other heterobilayer TMDs [29–31], the effect of interlayer electronic coupling is manifested in the band splittings at various critical points [32–34] such as K, Q, and Γ. Figure 1(b) shows the band structures

for MoS_2 from 1 monolayer (black curve) to $2H$-stacked bilayer (red curve) based on DFT at their natural state with $d = 0.62$ nm for the bilayer. Figure 1(c) shows the calculated band structure for the bilayer at a reduced interlayer spacing of 0.58 nm (see Fig. S1 in the Supplemental Material [35] for other d; also see Refs. [36–47]). The critical points of interest are K_V, Q_C, and Γ_V. Note that interlayer coupling at K_C is zero in the $2H$ stacking due to symmetry [19,20]. An increase in interlayer coupling will lead to an increase in energy splitting at these critical points [32–34]. At K_V, the energy separation between X_A and X_B excitons in the DR spectrum can be used to determine the d dependence of interlayer coupling [20]. The PL transition X_I from the lower Q_C state and the upper Γ_V state (an indirect transition) can be used to determine the d dependence of interlayer coupling at Q_C and Γ_V. Some early studies have reported pressure tuning of the band gap in bilayer MoS_2 and WSe_2 up to $\sim2-5$ GPa [48–50], indicating that interlayer coupling indeed depends on interlayer spacing. Here, we quantitatively determine coupling strength at various critical points, in which the magnitude and exponential dependence of t are independently demonstrated. Our results are particularly useful for vdW bilayers consisting of monolayers with different chalcogen atoms such as MoS_2/WSe_2, where the lattice corrugation and/or structure reconstruction effects can result in a more than 20% modulation of the vdW gap [29].

Experimentally, we exfoliate the MoS_2 sample directly onto the diamond surface [Figs. 1(d) and 1(e)], where the monolayer, bilayer, and bulk regions can be identified by optical contrast and second harmonic generation measurements. The compressive pressure is uniformly transferred by the inert gas Ne medium. Due to the weak interlayer vdW force, the applied pressure leads to much greater compression along the out of plane direction [51], generating a quasivertical compressive strain on the 2D sample and resulting in a reduced interlayer spacing d. We use the lattice parameters obtained by x-ray diffraction (XRD) of thicker MoS_2 samples under pressure [51] to convert the pressure dependence to the interlayer spacing dependence.

Exciton resonances in MoS_2 monolayers and bilayers occur at the K valley and exhibit large oscillator strength. As shown in Fig. 2(a), for a monolayer MoS_2, the spin splittings of the conduction band ($2\lambda_C$) and valence band ($2\lambda_V$) result from the spin-orbit coupling of the transition metal atoms [38,52,53]. The band splitting for bilayer and multilayer systems is further enhanced by the interlayer coupling, which is determined by the stacking configuration, band alignment, and valley spin [19,20]. For a $2H$-stacked bilayer [Fig. 2(b)], the coupling strength is zero (finite) for the conduction (valence) band edge [19,20]. In this context, the valence band splitting of the bilayer becomes $2\sqrt{\lambda_V^2 + t^2}$, which can be accessed optically. For example, two excitonic absorptions of the K valley (known as X_A and X_B excitons) are typically observed in the DR spectra [54–56]. Since $2\lambda_v$ is much larger than $2\lambda_c$ [38,52,53], the energy difference between two bright excitons $\Delta E \equiv X_B - X_A$ becomes a good measure of the valence band splitting $2\lambda_v$ ($2\sqrt{\lambda_V^2 + t^2}$) for monolayer (bilayer) MoS_2 (also see Note S1 in the Supplemental Material [35]).

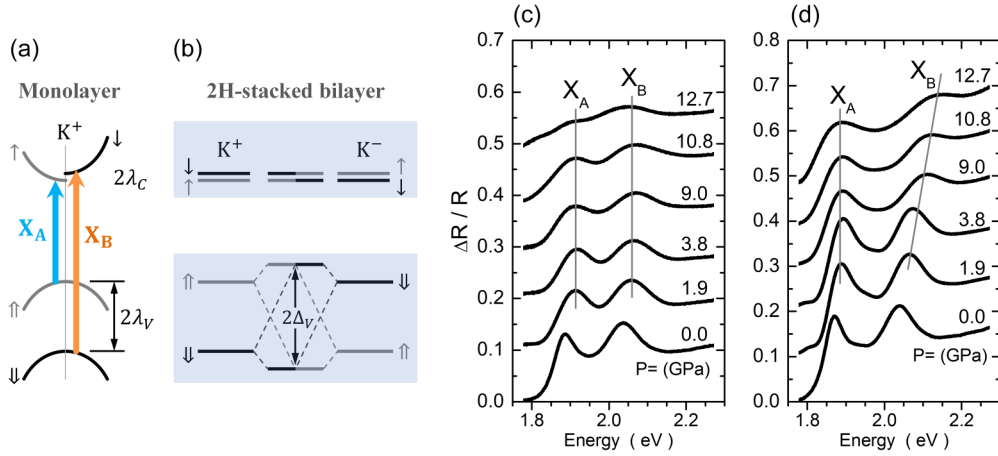Figures 2(c) and 2(d) show the DR spectra of monolayer and bilayer MoS_2 with applied compressive pressure,

FIG. 2. Pressure tuning of interlayer hopping integral at K valley. (a) Schematic showing the spin-allowed optical transitions (X_A and X_B) at the K^+ valley of monolayer MoS$_2$. The spin splitting of the conduction band ($2\lambda_C$) is much smaller than that of the valence band ($2\lambda_V$). (b) Schematic showing the interlayer hybridization of a 2H-stacked bilayer, in which the valence band splitting is enhanced ($2\Delta_V > 2\lambda_V$). Note that the interlayer hopping is allowed (forbidden) at the valence (conduction) band edge. (c), (d) DR spectra of the monolayer (c) and bilayer (d) MoS$_2$ under applied pressure. The spectra have been shifted vertically for clarity.

respectively. While ΔE ($=2\lambda_V$) of the monolayer is nearly independent of pressure, we find that ΔE ($=2\sqrt{\lambda_V^2 + t^2}$) of the bilayer increases significantly with the applied pressure, demonstrating that t is increasing. Figure 3(a) summarizes the pressure-dependent ΔE. Under applied pressure, the exciton energy difference ΔE of bilayer MoS$_2$ exhibits a nonlinear increase, while that of monolayer MoS$_2$ remains almost unchanged. The significant difference between them demon-

strates the pressure-dependent interlayer electronic coupling. For the monolayer sample, we notice that there are rigid X_A and X_B peak blueshifts ($\sim$20 meV) between zero and 1.9 GPa, which may be caused by strain-induced changes in band gap energy [51]. However, since our approach relies on energy difference, the influence of band gap energy has been largely eliminated. Based on the model, we extracted the coupling strength $t^{(K_V)}$ as a function of pressure, as displayed in Fig. 3(b) (also see Note S2 in the Supplemental Material [35]). At the highest applied pressure (12.7 GPa), we determined a coupling strength $t^{(K_V)} = 101$ meV, which is $\sim$280% greater than the value found at zero pressure ($t^{(K_V)} = 36$ meV). We also observe that $t^{(K_V)}$ exhibits an increasing slope at larger pressures.

Here we use the lattice parameters obtained by XRD of the thicker MoS$_2$ sample under pressure [51] to convert the pressure dependence to the d dependence, as shown in Fig. 3(c). In Fig. 3(d), we compare the experimental results (dots) with the spacing-dependent t extracted from the band structure calculations (blue line, DFT-1). In this calculation, we only change the interlayer spacing d and keep the in-plane lattice as a constant. It is clear that the coupling strength $t^{(K_V)}$ exhibits an exponential growth as a function of d. The results are fitted by an exponential function $t^{(K_V)} = t_0^{(K_V)} e^{-(d-d_0)/\lambda_0^{(K_V)}}$, with the equilibrium spacing $d_0 = 0.6165$ nm. We determine $t_0^{(K_V)} = 34$ meV (42 meV) and $\lambda_0^{(K_V)} = 0.046$ nm (0.070 nm) for the experimental (DFT-1) data. The discrepancy between the experimental and DFT results cannot be neglected; especially the fact that the decay length differs by about 34% (also see Tables S1 and S2 in the Supplemental Material [35]).

We realize that this difference arises from the effect of in-plane lattice compression, which occurs simultaneously when hydrostatic pressure is applied [51]. Based on the XRD data, we include both the in-plane and out of plane lattice compression in the calculation (red line, DFT-2). Clearly, after considering the effect of in-plane lattice compression, the calculations fit the experimental data much better. We obtain
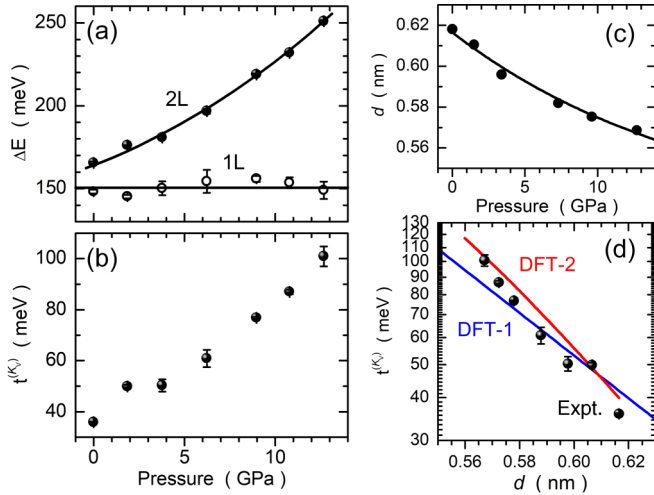

FIG. 3. Determination of the spacing-dependent coupling strength. (a) Pressure-dependent ΔE of monolayer and bilayer MoS$_2$. The dots are experimental data, and the solid lines are a guide to the eye. (b) Coupling strength t as a function of applied pressure, showing a 280% enhancement at 12.7 GPa compared to 0 GPa. (c) Pressure-dependent interlayer spacing d determined by XRD. (d) Comparison of experimentally determined (black dots) and DFT-calculated (blue/red curve) coupling strength as a function of d. In the calculation of DFT-1 (DFT-2), the compression of the in-plane lattice has not (has) been taken into account (see Figs. S1 and S2 in the Supplemental Material [35] for band structures).
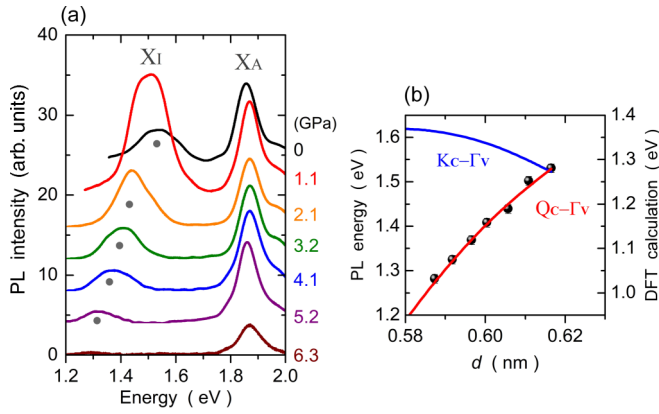
FIG. 4. Pressure tuning of the indirect gap. (a) PL spectra of bilayer MoS_2 under applied compressive pressure. The indirect gap X_I shows a significant redshift at high pressure. (b) A comparison of indirect gap measured by PL (dots) with the predicted evolution of the $E_{Q\Gamma}$ and $E_{K\Gamma}$ gap, showing excellent agreement with the energy evolution of the $E_{Q\Gamma}$ gap (red curve). The spacing dependence of $t^{(\Gamma v)}$ and $t^{(Q_C)}$ extracted from DFT calculation can be found in Fig. S4 in the Supplemental Material [35].

parameters of $t_0^{(K_V)} = 41$ meV and $\lambda_0^{(K_V)} = 0.054$ nm, which are only ∼15% different from the experimental data. Therefore, our results demonstrate that both in-plane and out of plane lattice compression can enhance the interlayer coupling strength, with the latter playing a major role. The reason can be readily understood from the view of orbital wave function overlap: Both in-plane and out of plane compression can bring the Mo atoms of the adjacent layer closer, resulting in higher wave function overlap and greater coupling strength.

We further evaluate the coupling strength at other valleys using the pressure-dependent PL spectra of bilayer MoS_2 [Fig. 4(a)]. The PL spectra feature two peaks, one from the direct K-K exciton and another from the indirect exciton X_I [26,27]. In stark contrast to the nearly unchanged K-K exciton (X_A) energy, the indirect exciton X_I exhibits a significant redshift of ∼240 meV from zero to 6.3 GPa. The PL redshift indicates the shrinkage of the indirect gap under pressure. At pressure higher than 6.3 GPa, the X_I indirect exciton emission is no longer detectable. After converting to the interlayer distance dependence, the indirect exciton transition energy as a function of interlayer distance, X_I vs d, is plotted in Fig. 4(b). Also shown are DFT calculations for the Q_C-Γ_V transition (red curve) and K_C-Γ_V transition (blue curve) as a function of interlayer distance. Interestingly, the energy redshift of X_I vs d shows excellent agreement with the Q_C-Γ_V transition except for an apparent offset of ∼0.25 eV. This offset is not surprising since DFT calculations often underestimate the band gap [57]. Due to the close energy of K_C and Q_C points in the conduction band, the PL emission of the indirect gap in bilayer MoS_2 has been under debate [26,27]. Our results show that indirect PL emission is mainly from Q_C-Γ_V excitons [48]. Under applying compressive pressure, the lifting up of the Γ_V point and the pushing down of the Q_C point both contribute to the shrinkage of the indirect gap [Figs. 1(b) and 1(c)].

Our optical spectroscopy measurements do not independently determine the interlayer coupling at Q_C and Γ_V. Rather,

it is a combined effect of Q_C and Γ_V as a function of d. However, given the fact the experimental result of X_I vs d shows excellent agreement with the calculated result for the Q_C-Γ_V transition, we can conclude that the calculated results for the interlayer coupling at Q_C and Γ_V are individually accurate (also see Tables S1 and S2 in the Supplemental Material [35]). In this context, we are able to extract the coupling strength of the Q_C and Γ_V points from the DFT calculations using the 2×2 Hamiltonian. As shown in Fig. S4 in the Supplemental Material [35], the obtained results also exhibit an exponential dependence on d and can be fitted by an exponential function, with extracted $\lambda_0^{(\Gamma_V)} = 0.067$ nm ($\lambda_0^{(Q_C)} = 0.108$ nm) for $t^{(\Gamma_V)}$ ($t^{(Q_C)}$). When the pressure changes from zero to 6.3 GPa, we determine that $t^{(\Gamma_V)}$ changes from 335 to 522 meV and $t^{(Q_C)}$ from 192 to 253 meV.

In Tables S1 and S2 in the Supplemental Material [35], we summarize and compare the experimental results with the DFT calculations. We conclude that the coupling strength (decay length) of Γ_V and Q_C are larger (longer) than that of K_V. This valley-dependent coupling strength is due to the fact that the interlayer hopping integral is affected by the p_z orbitals of the chalcogen atoms. Since the atomic distances between the inner chalcogen atoms of adjacent layers are the shortest, the large orbital wave function overlap leads to significant p_z-p_z hybridization [58]. Our results show that the coupling strength is indeed correlated to the p_z-orbital component of the critical point, i.e., p_z-orbital components of Γ_V, Q_C, and K_V points are 28%(Γ_V) > 11%(Q_C) > 0%(K_V), which leads to $t_0^{(\Gamma_V)} > t_0^{(Q_C)} > t_0^{(K_V)}$. In addition, the decay length exhibits a trend of $\lambda_0^{(\Gamma_V)}, \lambda_0^{(Q_C)} > \lambda_0^{(K_V)}$, which can also be understood by p_z-p_z hybridization. Since the wave function of p_z orbitals elongates in the z direction, a less sensitive d dependence can be expected, which leads to longer decay lengths at Γ_V and Q_C than that at K_V. On the contrary, the states at K_V comprise transition metal $d_{x^2-y^2}$, d_{xy} as the majority orbital, and chalcogen p_x, p_y as the minority orbital (see Table S3 in the Supplemental Material [35]), leading to a rapidly decaying wave function along the z direction and a shorter decay length.

In conclusion, our experiments firmly establish the exponential dependence of the electronic coupling on the interlayer spacing at various critical points of bilayer MoS_2. In particular, we quantitatively determine the coupling strengths of the Γ_V, Q_C, and K_V points, as well as their interlayer spacing dependence. We experimentally demonstrate that, due to the increased overlap of atomic orbital wave functions, interlayer coupling strength can be enhanced by both in-plane and out of plane lattice compression, with the latter playing a major role. By measuring the absorption of X_A and X_B excitons, $t^{(K_V)}$ and its d dependence are independently determined, which are believed to be free from other factors such as band gap and exciton binding energy. In addition, we demonstrate that by applying a moderate pressure of 12.7 GPa, the interlayer K-valley coupling can achieve a 280% enhancement over that in natural bilayers. Through the PL measurement of indirect excitons, we also determine the d dependence of $t^{(\Gamma_V)}$ and $t^{(Q_C)}$. These results have important implications for vdW heterostructures. Tuning the magic angle in twisted bilayer graphene through hydrostatic pressure has recently been demonstrated [21]. One therefore expects similar tunability can be achieved in twisted bilayer WSe_2 [11,12]. Most

importantly, in the current topic of moiré designing of vdW hetero- and homobilayers, the shallow moiré potential depth has limited the observation of novel physics at low temperatures. A factor of 3 enhancement in modulation amplitude will liberate this limitation, thus profoundly impacting the applications of the vdW bilayer system [59] in quantum information (e.g., quantum simulator) and other quantum phenomena.

[1] A. K. Geim and I. V. Grigorieva, Van der Waals heterostructures, Nature (London) **499**, 419 (2013).

[2] L. A. Ponomarenko, R. V. Gorbachev, G. L. Yu, D. C. Elias, R. Jalil, A. A. Patel, A. Mishchenko, A. S. Mayorov, C. R. Woods, J. R. Wallbank, M. Mucha-Kruczynski, B. A. Piot, M. Potemski, I. V. Grigorieva, K. S. Novoselov, F. Guinea, V. I. Fal'ko, and A. K. Geim, Cloning of Dirac fermions in graphene superlattices, Nature (London) **497**, 594 (2013).

[3] C. R. Dean, L. Wang, P. Maher, C. Forsythe, F. Ghahari, Y. Gao, J. Katoch, M. Ishigami, P. Moon, M. Koshino, T. Taniguchi, K. Watanabe, K. L. Shepard, J. Hone, and P. Kim, Hofstadter's butterfly and the fractal quantum Hall effect in moiré superlattices, Nature (London) **497**, 598 (2013).

[4] B. Hunt, J. D. Sanchez-Yamagishi, A. F. Young, M. Yankowitz, B. J. LeRoy, K. Watanabe, T. Taniguchi, P. Moon, M. Koshino, P. Jarillo-Herrero, and R. C. Ashoori, Massive Dirac fermions and Hofstadter butterfly in a van der Waals heterostructure, Science **340**, 1427 (2013).

[5] R. V. Gorbachev, J. C. W. Song, G. L. Yu, A. V. Kretinin, F. Withers, Y. Cao, A. Mishchenko, I. V. Grigorieva, K. S. Novoselov, L. S. Levitov, and A. K. Geim, Detecting topological currents in graphene superlattices, Science **346**, 448 (2014).

[6] H. Yu, G.-B. Liu, J. Tang, X. Xu, and W. Yao, Moiré excitons: From programmable quantum emitter arrays to spin-orbit-coupled artificial lattices, Sci. Adv. **3**, e1701696 (2017).

[7] J. C. W. Song and N. M. Gabor, Electron quantum metamaterials in van der Waals heterostructures, Nat. Nanotechnol. **13**, 986 (2018).

[8] Y. Cao, V. Fatemi, S. Fang, K. Watanabe, T. Taniguchi, E. Kaxiras, and P. Jarillo-Herrero, Unconventional superconductivity in magic-angle graphene superlattices, Nature (London) **556**, 43 (2018).

[9] Y. Cao, V. Fatemi, A. Demir, S. Fang, S. L. Tomarken, J. Y. Luo, J. D. Sanchez-Yamagishi, K. Watanabe, T. Taniguchi, E. Kaxiras, R. C. Ashoori, and P. Jarillo-Herrero, Correlated insulator behaviour at half-filling in magic-angle graphene superlattices, Nature (London) **556**, 80 (2018).

[10] A. L. Sharpe, E. J. Fox, A. W. Barnard, J. Finney, K. Watanabe, T. Taniguchi, M. A. Kastner, and D. Goldhaber-Gordon, Emergent ferromagnetism near three-quarters filling in twisted bilayer graphene, Science **365**, 605 (2019).

[11] L. Wang, E.-M. Shih, A. Ghiotto, L. Xian, D. A. Rhodes, C. Tan, M. Claassen, D. M. Kennes, Y. Bai, B. Kim, K. Watanabe, T. Taniguchi, X. Zhu, J. Hone, A. Rubio, A. Pasupathy, and C. R. Dean, Correlated electronic phases in twisted bilayer transition metal dichalcogenides, Nat. Mater. **19**, 861 (2020).

[12] L. An, X. Cai, D. Pei, M. Huang, Z. Wu, Z. Zhou, J. Lin, Z. Ying, Z. Ye, X. Feng, R. Gao, C. Cacho, M. Watson, Y. Chen, and N. Wang, Interaction effects and superconductivity signatures in twisted double-bilayer WSe_2, Nanoscale Horiz. **5**, 1309 (2020).

[13] K. L. Seyler, P. Rivera, H. Yu, N. P. Wilson, E. L. Ray, D. G. Mandrus, J. Yan, W. Yao, and X. Xu, Signatures of moiré-trapped valley excitons in $MoSe_2$/WSe_2 heterobilayers, Nature (London) **567**, 66 (2019).

[14] K. Tran, G. Moody, F. Wu, X. Lu, J. Choi, K. Kim, A. Rai, D. A. Sanchez, J. Quan, A. Singh, J. Embley, A. Zepeda, M. Campbell, T. Autry, T. Taniguchi, K. Watanabe, N. Lu, S. K. Banerjee, K. L. Silverman, S. Kim *et al.*, Evidence for moiré excitons in van der Waals heterostructures, Nature (London) **567**, 71 (2019).

[15] C. Jin, E. C. Regan, A. Yan, M. Iqbal Bakti Utama, D. Wang, S. Zhao, Y. Qin, S. Yang, Z. Zheng, S. Shi, K. Watanabe, T. Taniguchi, S. Tongay, A. Zettl, and F. Wang, Observation of moiré excitons in WSe_2/WS_2 heterostructure superlattices, Nature (London) **567**, 76 (2019).

[16] E. M. Alexeev, D. A. Ruiz-Tijerina, M. Danovich, M. J. Hamer, D. J. Terry, P. K. Nayak, S. Ahn, S. Pak, J. Lee, J. I. Sohn, M. R. Molas, M. Koperski, K. Watanabe, T. Taniguchi, K. S. Novoselov, R. V. Gorbachev, H. S. Shin, V. I. Fal'ko, and A. I. Tartakovskii, Resonantly hybridized excitons in moiré superlattices in van der Waals heterostructures, Nature (London) **567**, 81 (2019).

[17] L. Zhang, Z. Zhang, F. Wu, D. Wang, R. Gogna, S. Hou, K. Watanabe, T. Taniguchi, K. Kulkarni, T. Kuo, S. R. Forrest, and H. Deng, Twist-angle dependence of moiré excitons in WS_2/$MoSe_2$ heterobilayers, Nat. Commun. **11**, 5888 (2020).

[18] Y. Bai, L. Zhou, J. Wang, W. Wu, L. J. McGilly, D. Halbertal, C. F. B. Lo, F. Liu, J. Ardelean, P. Rivera, N. R. Finney, X.-C. Yang, D. N. Basov, W. Yao, X. Xu, J. Hone, A. N. Pasupathy, and X.-Y. Zhu, Excitons in strain-induced one-dimensional moiré potentials at transition metal dichalcogenide heterojunctions, Nat. Mater. **19**, 1068 (2020).

[19] Q. Tong, H. Yu, Q. Zhu, Y. Wang, X. Xu, and W. Yao, Topological mosaics in moiré superlattices of van der Waals heterobilayers, Nat. Phys. **13**, 356 (2017).

[20] W.-T. Hsu, B.-H. Lin, L.-S. Lu, M.-H. Lee, M.-W. Chu, L.-J. Li, W. Yao, W.-H. Chang, and C.-K. Shih, Tailoring excitonic states of van der Waals bilayers through stacking configuration, band alignment, and valley spin, Sci. Adv. **5**, eaax7407 (2019).

[21] M. Yankowitz, S. Chen, H. Polshyn, Y. Zhang, K. Watanabe, T. Taniguchi, D. Graf, A. F. Young, and C. R. Dean, Tuning superconductivity in twisted bilayer graphene, Science **363**, 1059 (2019).

[22] J. Xia, J. Yan, Z. Wang, Y. He, Y. Gong, W. Chen, T. C. Sum, Z. Liu, P. M. Ajayan, and Z. Shen, Strong coupling and pressure engineering in WSe$_2$-MoSe$_2$ heterobilayers, Nat. Phys. **17**, 92 (2021).

[23] W. Zhao, E. C. Regan, D. Wang, C. Jin, S. Hsieh, Z. Wang, J. Wang, Z. Wang, K. Yumigeta, M. Blei, K. Watanabe, T. Taniguchi, S. Tongay, N. Y. Yao, and F. Wang, Dynamic tuning of moiré excitons in a WSe$_2$/WS$_2$ heterostructure via mechanical deformation, Nano Lett. **21**, 8910 (2021).

[24] M. Zhu, Z. Zhang, T. Zhang, D. Liu, H. Zhang, Z. Zhang, Z. Li, Y. Cheng, and W. Huang, Exchange between interlayer and intralayer exciton in WSe$_2$/WS$_2$ heterostructure by interlayer coupling engineering, Nano Lett. **22**, 4528 (2022).

[25] L. J. McGilly, A. Kerelsky, N. R. Finney, K. Shapovalov, E.-M. Shih, A. Ghiotto, Y. Zeng, S. L. Moore, W. Wu, Y. Bai, K. Watanabe, T. Taniguchi, M. Stengel, L. Zhou, J. Hone, X.-Y. Zhu, D. N. Basov, C. Dean, C. E. Dreyer, and A. N. Pasupathy, Visualization of moiré superlattices, Nat. Nanotechnol. **15**, 580 (2020).

[26] A. M. van der Zande, J. Kunstmann, A. Chernikov, D. A. Chenet, Y. You, X. Zhang, P. Y. Huang, T. C. Berkelbach, L. Wang, F. Zhang, M. S. Hybertsen, D. A. Muller, D. R. Reichman, T. F. Heinz, and J. C. Hone, Tailoring the electronic structure in bilayer molybdenum disulfide via interlayer twist, Nano Lett. **14**, 3869 (2014).

[27] K. Liu, L. Zhang, T. Cao, C. Jin, D. Qiu, Q. Zhou, A. Zettl, P. Yang, S. G. Louie, and F. Wang, Evolution of interlayer coupling in twisted molybdenum disulfide bilayers, Nat. Commun. **5**, 4966 (2014).

[28] P.-C. Yeh, W. Jin, N. Zaki, J. Kunstmann, D. Chenet, G. Arefe, J. T. Sadowski, J. I. Dadap, P. Sutter, J. Hone, and R. M. Osgood Jr., Direct measurement of the tunable electronic structure of bilayer MoS$_2$ by interlayer twist, Nano Lett. **16**, 953 (2016).

[29] C. Zhang, C.-P. Chuu, X. Ren, M.-Y. Li, L.-J. Li, C. Jin, M.-Y. Chou, and C.-K. Shih, Interlayer couplings, moiré patterns, and 2D electronic superlattices in MoS$_2$/WSe$_2$ hetero-bilayers, Sci. Adv. **3**, e1601459 (2017).

[30] J. Kunstmann, F. Mooshammer, P. Nagler, A. Chaves, F. Stein, N. Paradiso, G. Plechinger, C. Strunk, C. Schüller, G. Seifert, D. R. Reichman, and T. Korn, Momentum-space indirect interlayer excitons in transition-metal dichalcogenide van der Waals heterostructures, Nat. Phys. **14**, 801 (2018).

[31] A. T. Hanbicki, H.-J. Chuang, M. R. Rosenberger, C. S. Hellberg, S. V. Sivaram, K. M. McCreary, I. I. Mazin, and B. T. Jonker, Double indirect interlayer exciton in a MoSe$_2$/WSe$_2$ van der Waals heterostructure, ACS Nano **12**, 4719 (2018).

[32] X. Fan, D. J. Singh, and W. Zheng, Valence band splitting on multilayer MoS$_2$: Mixing of spin-orbit coupling and interlayer coupling, J. Phys. Chem. Lett. **7**, 2175 (2016).

[33] A. Kormányos, V. Zólyomi, V. I. Fal'ko, and G. Burkard, Tunable Berry curvature and valley and spin Hall effect in bilayer MoS$_2$, Phys. Rev. B **98**, 035408 (2018).

[34] A. O. Slobodeniuk, Ł. Bala, M. Koperski, M. R. Molas, P. Kossacki, K. Nogajewski, M. Bartos, K. Watanabe, T. Taniguchi, C. Faugeras, and M. Potemski, Fine structure of K-excitons in multilayers of transition metal dichalcogenides, 2D Mater. **6**, 025026 (2019).

[35] See Supplemental Material at http://link.aps.org/supplemental/10.1103/PhysRevB.106.125302, which includes a detailed description of materials and methods, experimental conditions, theoretical analysis, discussion, and Refs. [36–47].

[36] A. Dewaele, M. Torrent, P. Loubeyre, and M. Mezouar, Compression curves of transition metals in the Mbar range: Experiments and projector augmented-wave calculations, Phys. Rev. B **78**, 104102 (2008).

[37] E. Cappelluti, R. Roldán, J. A. Silva-Guillén, P. Ordejón, and F. Guinea, Tight-binding model and direct-gap/indirect-gap transition in single-layer and multilayer MoS$_2$, Phys. Rev. B **88**, 075409 (2013).

[38] A. Kormányos, G. Burkard, M. Gmitra, J. Fabian, V. Zólyomi, N. D. Drummond, and V. Fal'ko, $k \cdot p$ theory for two-dimensional transition metal dichalcogenide semiconductors, 2D Mater. **2**, 022001 (2015).

[39] K. Kim, M. Yankowitz, B. Fallahazad, S. Kang, H. C. P. Movva, S. Huang, S. Larentis, C. M. Corbet, T. Taniguchi, K. Watanabe, S. K. Banerjee, B. J. LeRoy, and E. Tutuc, Van der Waals heterostructures with high accuracy rotational alignment, Nano Lett. **16**, 1989 (2016).

[40] G. Kresse and J. Furthmüller, Efficient iterative schemes for *ab initio* total-energy calculations using a plane-wave basis set, Phys. Rev. B **54**, 11169 (1996).

[41] G. Kresse and J. Furthmüller, Efficiency of *ab-initio* total energy calculations for metals and semiconductors using a plane-wave basis set, Comput. Mater. Sci. **6**, 15 (1996).

[42] P. E. Blöchl, Projector augmented-wave method, Phys. Rev. B **50**, 17953 (1994).

[43] G. Kresse and D. Joubert, From ultrasoft pseudopotentials to the projector augmented-wave method, Phys. Rev. B **59**, 1758 (1999).

[44] J. P. Perdew, K. Burke, and M. Ernzerhof, Generalized Gradient Approximation Made Simple, Phys. Rev. Lett. **77**, 3865 (1996).

[45] H. J. Monkhorst and J. D. Pack, Special points for Brillouin-zone integrations, Phys. Rev. B **13**, 5188 (1976).

[46] M. Dion, H. Rydberg, E. Schröder, D. C. Langreth, and B. I. Lundqvist, Van der Waals Density Functional for General Geometries, Phys. Rev. Lett. **92**, 246401 (2004).

[47] J. Klimeš, D. R. Bowler, and A. Michaelides, Van der Waals density functionals applied to solids, Phys. Rev. B **83**, 195131 (2011).

[48] X. Dou, K. Ding, D. Jiang, and B. Sun, Transitions in monolayer and bilayer molybdenum disulfide using hydrostatic pressure, ACS Nano **8**, 7458 (2014).

[49] X. Dou, K. Ding, D. Jiang, X. Fan, and B. Sun, Probing spin-orbit coupling and interlayer coupling in atomically thin molybdenum disulfide using hydrostatic pressure, ACS Nano **10**, 1619 (2016).

[50] Y. Ye, X. Dou, K. Ding, D. Jiang, F. Yang, and B. Sun, Pressure-induced K-Λ crossing in monolayer WSe$_2$, Nanoscale **8**, 10843 (2016).

[51] A. P. Nayak, S. Bhattacharyya, J. Zhu, J. Liu, X. Wu, T. Pandey, C. Jin, A. K. Singh, D. Akinwande, and J.-F. Lin, Pressure-induced semiconducting to metallic transition in multilayered molybdenum disulphide, Nat. Commun. **5**, 3731 (2014).

[52] G.-B. Liu, W.-Y. Shan, Y. Yao, W. Yao, and D. Xiao, Three-band tight-binding model for monolayers of group-VIB transition metal dichalcogenides, Phys. Rev. B **88**, 085433 (2013).

[53] K. Kośmider, J. W. González, and J. Fernández-Rossier, Large spin splitting in the conduction band of transition metal dichalcogenide monolayers, Phys. Rev. B **88**, 245436 (2013).

[54] A. Splendiani, L. Sun, Y. Zhang, T. Li, J. Kim, C.-Y. Chim, G. Galli, and F. Wang, Emerging photoluminescence in monolayer MoS$_2$, Nano Lett. **10**, 1271 (2010).

[55] K. F. Mak, C. Lee, J. Hone, J. Shan, and T. F. Heinz, Atomically Thin MoS$_2$: A New Direct-Gap Semiconductor, Phys. Rev. Lett. **105**, 136805 (2010).

[56] W. Zhao, Z. Ghorannevis, L. Chu, M. Toh, C. Kloc, P.-H. Tan, and G. Eda, Evolution of electronic structure in atomically thin sheets of WS$_2$ and WSe$_2$, ACS Nano **7**, 791 (2013).

[57] J. K. Ellis, M. J. Lucero, and G. E. Scuseria, The indirect to direct band gap transition in multilayered MoS$_2$ as predicted by screened hybrid density functional theory, Appl. Phys. Lett. **99**, 261908 (2011).

[58] S. Fang, R. Kuate Defo, S. N. Shirodkar, S. Lieu, G. A. Tritsaris, and E. Kaxiras, *Ab initio* tight-binding Hamiltonian for transition metal dichalcogenides, Phys. Rev. B **92**, 205108 (2015).

[59] D. M. Kennes, M. Claassen, L. Xian, A. Georges, A. J. Millis, J. Hone, C. R. Dean, D. N. Basov, A. N. Pasupathy, and A. Rubio, Moiré heterostructures as a condensed-matter quantum simulator, Nat. Phys. **17**, 155 (2021).